Invited Comment

Two views at strained nanocrystals from the opposite sides of spatial resolution limit

Anatoly I Frenkel

Physics Department, Yeshiva University, 245 Lexington Avenue, New York, NY 10016, USA

E-mail: anatoly.frenkel@yu.edu

CrossMark

Abstract

From the unique paths charted by two synchrotron communities to the challenges they both faced, this article compares the two approaches: x-ray scattering and x-ray absorption spectroscopy towards the goal of strain determination in nanometer-scale metal clusters, and the special role Ian Robinson's work played in the process.

Keywords: nanocrystals, EXAFS, coherent x-ray diffraction

(Some figures may appear in colour only in the online journal)

1. Introduction

Physics and lyrics, fire and ice, love and hatred are often perceived as *yin* and *yang*, the two sides of a man that are contradictory but also complementary to each other. Interestingly, among the user communities of synchrotrons light sources, many scientists are still divided across the lines of a particular technique (e.g., scattering versus spectroscopy) they practised during their formative years in graduate schools. Despite our scientific interests in multidisciplinary fields that call for combinations of multiple methods, we are often informally referred to by our colleagues as diffraction, extended x-ray absorption fine structure (EXAFS) or microscopy folks… With respect to the Bragg diffraction and x-ray absorption structure analysis methods the litmus test that detects either scattering or absorption 'mentality' is how we think about the three-dimensional positions of atomic species in our samples. In Bragg diffraction, coherent scattering originates from periodic arrangement of atoms in a sample that produces constructive interference and thus a Bragg peak at a certain point in reciprocal space. From analysis of Bragg peaks, average positions of atoms in the periodic lattice (in one, two or three dimensions) can be obtained. In EXAFS, the interference effect is between the outgoing photoelectron wave, emitted from the atom that absorbed an x-ray photon, and the incoming wave that underwent scattering by neighboring atoms in the vicinity of the absorber. Due to the

inherent many-body nature of the interference, EXAFS probes the distances between the x-ray absorber atom and the atoms along the photoelectron scattering paths and thus lacks any sensitivity to the individual atom positions. It is because of that difference the two techniques, Bragg diffraction and EXAFS, are best used when their strengths are best exploited: the former, for structural refinement of systems where average periodic lattice exists, and the latter, in the systems with disorder, where the average structure and local structure are different or the average structure does not exist at all.

Ian Robinson's research of strained nanocrystals by coherent x-ray diffraction (CXD) is an example where the strengths of the Bragg diffraction are tested at many limits at once: at small crystalline sizes, where coherent scattering signals are relatively weak and thus difficult to detect, and at large disorder due to the proximity of the surface. In addition, in order to produce a real space image from the measured data, it is required to retrieve the phase of coherently scattered x-rays, an obstacle of x-ray crystallography known as the phase problem [1]. Ian transformed the field by extending the limits of CXD techniques to enable detection of strain in systems as small as 10 nm in size, and, if electron diffraction is considered, down to about 3–5 nm [2]. Breaking the spatial resolution limit of a few tens of nm for strain determination seems to be a challenging task for x-ray diffraction, even at new generation synchrotron sources. On the other hand, the nm-scale strains, i.e., those on the 'other side' of the spatial

resolution limit of CXD methods, are an important attribute of mono- and bimetallic heterogeneous catalysts that presently cannot be detected by x-ray diffraction techniques (and strain measurements by electron diffraction in such systems can be presently done *ex situ* only which is a serious limitation in their mechanistic studies [2]). The particles in the nm-scale range have a rich variety of structures, shapes, support interactions, adsorbate coverages and degrees of order [3–6], all of which are considered important catalytic descriptors and correlate with each other, hence, hindering their investigations [7]. Strain is also mentioned as an important factor in catalytic activity of metal particles [8–12, 13].

The good news is that, where scattering methods start to lose their analytic capabilities for strain determination (that is, near the spatial resolution limit for CXD), x-ray absorption methods rise to the challenge, as will be shown in this Comment, but the transition across the limit is anything but smooth. One reason for that is the different emphases on the local and average structures that the members of the two communities (absorption and average) make when approaching the same problem of strain determination. Marshall Stoneham, whom I met at the UCL while visiting Ian there, once wrote about many challenges in understanding nanoscale behavior, that applies to the above challenge as well: '*The temptation for those used to macroscopic theory is to believe nanoscience is miniaturized macroscience; for those used to the atomic scale, the temptation is to believe that it suffices to extend familiar atomistic ideas*' [14].

In this Comment I will visit each 'camp' and take a peek over the barrier separating the two regimes (and the two approaches) and will compare the methods pioneered by Ian for studying strained nanoparticles with sizes above the CXD resolution limit, with those developed for strained nanoparticles on the other side of the limit (less than 3–5 nm in size). To keep focus on the CXD methods developed by Ian, and for the sake of brevity, I will not discuss other scattering methods, such as diffuse scattering or pair distribution function techniques. I will first overview methods developed by Ian Robinson and his collaborators for surface strain investigation. In what follows I will present a view from an x-ray spectroscopy perspective at the strain problem.

2. Ian Robinson's research of surface strain in nanocrystals

Coherent XRD occurs when the size of the sample is smaller than the coherence of the x-ray beam [15]. When the crystal is exposed to coherent beams, its diffraction pattern will show interference effects in addition to those giving rise to Bragg diffraction peaks. Those interference effects can arise from facets, hence, enabling the full three-dimensional (3D) imaging of the objects. The interference effects are modified in the presence of strain and thus reveal information about the atomic displacement field $\vec{u}$ [16]. Examples of 1D, 2D and 3D strain fields are assembled from Ian Robinson's papers and are shown in figure 1. Quantitatively, the information about the strain is extracted from the experimental data due to the

inversion symmetry breaking of a diffraction pattern about the Bragg point, because of the presence of strain [17]. Because of the lack of inversion symmetry, the Fourier transform of the diffraction pattern is complex, possessing phase structure in real space [17]. Inversion of the diffraction pattern with this additional structure can be done by an 'oversampling' [18, 19], normally, impossible for macroscopic, strain-free, crystals because all the intensity is concentrated in Bragg peaks [20].

More than a decade ago, Ian and colleagues pointed out that third generation synchrotron radiation sources produce beams with coherence lengths in the range of 10 μm (transverse) and 1 μm (longitudinal), hence, the strain distribution can be measured within micron-sized crystals [15, 16]. Sub-micron coherence lengths of the new synchrotron sources are now available with sufficient flux, to make such experiments practical [21, 22]. In that case, spatial distribution of strain within a nanometer-sized crystal can be obtained. In the first article that demonstrated strains in sub-micron crystals, 100 nm crystals were used [15]. In subsequent articles, more examples are shown, for particles ranging from hundreds to tens nm in diameter [23]. The latter advances were achieved using high-quality optics suitable for the hard x-ray regime, such as a Fresnel zone plate that provides 50 nm spatial resolution [24]. The resolution limit of this method can be improved in the future with the use of the coherent x-ray sources, such as an x-ray free-electron laser [17].

3. Lowering the resolution limit: coherent electron diffraction studies of nm-scale particles

For smaller particles, the photon-hungry CXD method is challenging, but coherent electron diffraction can be used instead of x-rays. Huang *et al* demonstrated, using coherent electron diffraction, that the surface of 4 nm Au nanoparticle exhibits bond length contraction [2]. Coherent electron diffraction method is based on the same principle as the CXD: the displacements of atoms from periodic lattice sites in the nanocrystals translate into the local asymmetry around the Bragg peaks. Using molecular dynamic simulations, they obtained that the strain propagated into the interior of the nanoparticle to the depth of two atomic layers (figure 2). That estimate was obtained using the guidance of the continuum elastic theory that was used by Ian Robinson and colleagues in their work using CXD [23].

The average intensity decays rapidly away from the center of the Bragg peak, eventually reaching the background level of the detector. This radial cut-off determines the spatial resolution of the resulting real-space image. This is limited, in practice, by the counting statistics, but more by the stability of the sample and instrument, as well as the brightness of the x-ray source. At present, the typical resolution of these experiments is around 40 nm, but is expected to improve to 10 nm as the technique develops [25]. For even smaller crystals the x-ray scattering techniques cannot be used for strain determination. Particularly when using a focused beam, strong radiation forces can cause the small samples to move
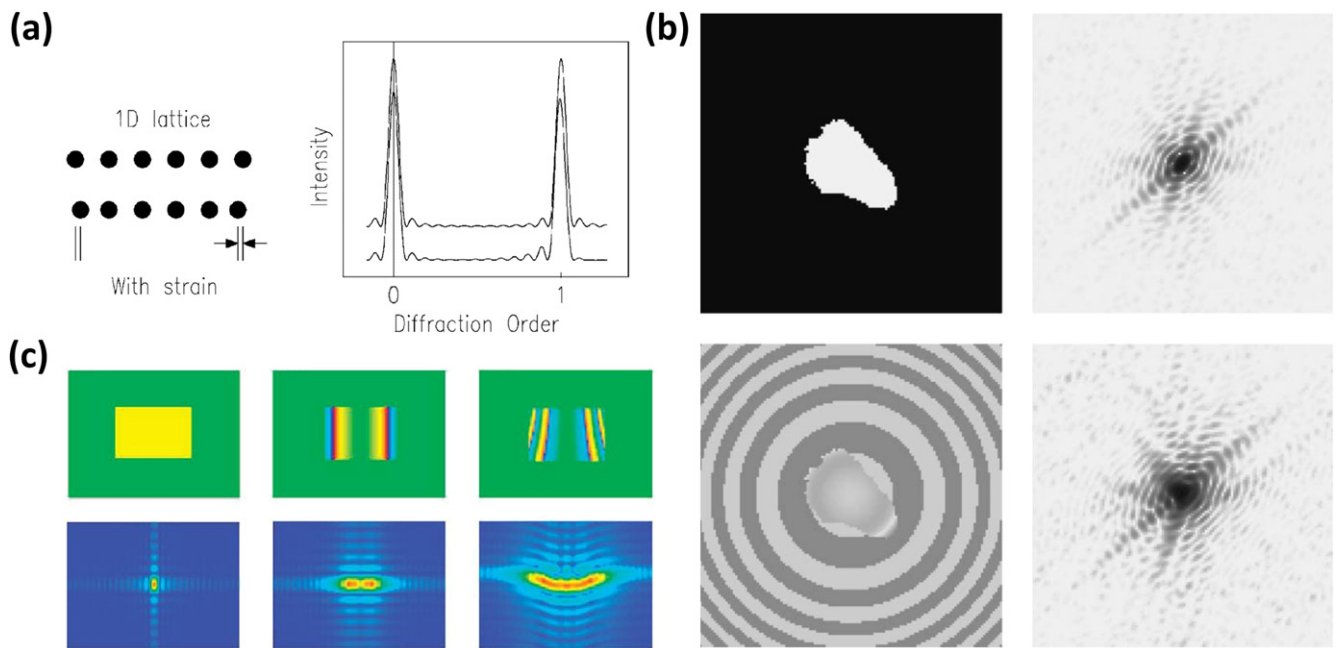
Figure 1. Illustration of the effects of strain on the diffraction from a 1D (a), 2D (b) and 3D (c) crystal. (a) The finite-sized array of atoms gives a diffraction pattern in the form of a slit function. When strain is introduced by displacing atoms as shown in the lower trace, the diffraction pattern becomes asymmetric around its first-order maximum (reproduced with permission from [15]). (b) Illustration of the effects of strain on the diffraction from a 2D crystal. The upper panel shows an unstrained object and its calculated coherent diffraction pattern. The lower panel is the same with the addition of a real-space strain increasing quadratically with radius from the center of the object. The alternate circular shading denotes positions for which the phase lies between 0 and π or between π and 2π (reproduced with permission from [15]). (c) Simulated 3D rectangular parallelepiped objects with parabolic phase distributions (upper panel) and the corresponding calculated diffraction patterns (lower level). The introduced parabolic phase functions are shown on a color wheel with green representing $\phi = 0$, blue $\phi = -\pi$ and red $\phi = \pi$. The amplitudes of the calculated diffraction patterns are shown on a standard rainbow color scale (reproduced with permission from [16]).
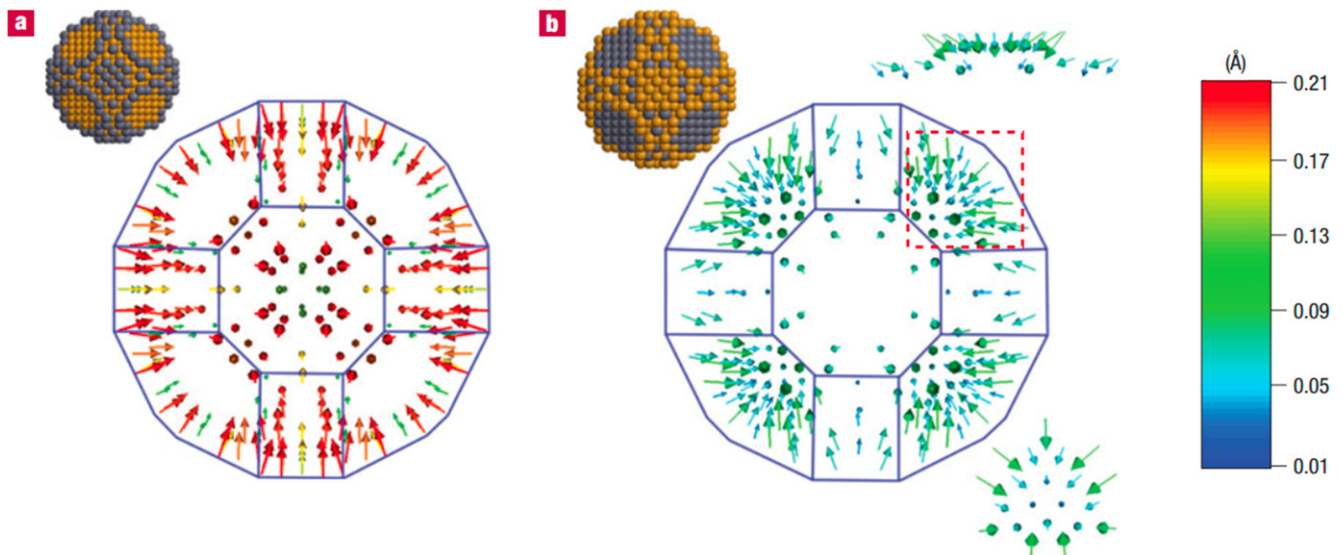

Figure 2. Surface atom contraction obtained from the molecular dynamic simulation of Au nanoparticles. Surface atom displacements shown as vectors for atoms possessing a coordination number less than 9 (a) and equal to 9 (b). The upper right inset in b shows a magnified {111} facet viewed parallel to the facet, whereas the lower right inset shows the same facet viewed normal to the facet (which is tilted slightly to avoid atoms on the other facets). The magnitudes of the displacements are rendered using colors. The corresponding atoms in the nanocrystal model are shown in the inset at the top left corner; the atoms whose displacements are shown are colored in gray. Both maps have the same display scale in the magnitude of displacement. Reproduced with permission from [2].
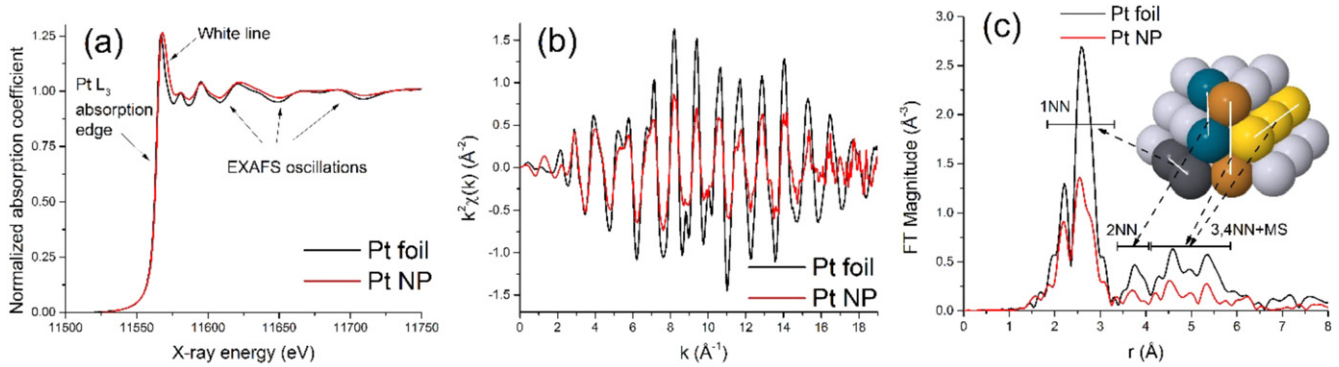
Figure 3. Raw EXAFS data are shown in energy-(a), k-(b), and r-space (c) for Pt nanoparticles supported on high surface area γ-Al$_2$O$_3$ substrate and for bulk Pt. The inset in (c) shows a model of a truncated cuboctahedral cluster and different groups of atomic arrangements that contribute to different peaks in r-space. Reproduced with permission from [3].

around in the beam. To avoid sample-stability problems, nanocrystals can be grown directly on substrates or in confined geometries [25]. With electron scattering, the spatial resolution limit can be lowered to 4 nm but the challenges of a different nature (e.g., a current inability to do *in situ* experiments) limit the range of applications of TEM-based electron diffraction technique for strain determination. An alternative is to use techniques based on the x-ray absorption spectroscopy, namely, EXAFS, as described in greater detail below.

4. Determination of strain by EXAFS spectroscopy

EXAFS is among the best techniques for comprehensive investigations of finite size effects on electronic structure, geometry and bond dynamics in metal nanoparticles of the characteristic sizes of less than 5 nm [26–29]. With this method, fine structure in the resonance region of the x-ray absorption coefficient (called the absorption edge) is measured in either a transmission or fluorescence detection mode. The edge region (within 30 eV below to 40 eV above the edge), known as the x-ray absorption near-edge structure, contains information about the electronic structure and local geometry of the absorbing atom and its nearest neighbors. The post-edge region that extends from ~40 eV to between 1000–1500 eV (depending on the system) past the edge contains an oscillatory signal and is known as the EXAFS [30]. The origin of the fine structure is the interference between the incoming and scattered photoelectron waves. The interference pattern contains quantitative information about the local atomic environment in the proximity of the absorbing atom. The frequency of these oscillations can be quantitatively related to the distances between the absorbing atom and atoms within a given coordination shell around it (figure 3). The EXAFS signal therefore contains information about interatomic distances and their disorder (due to the static and dynamic displacements of all atoms from their average positions). The amplitude of these oscillations correlates with the number of neighboring atoms of a given type.

The oscillatory part of the absorption coefficient—$\chi(k)$—contains the sum of all contributions $\chi_i(k)$ from

groups of neighbor atoms at approximately equal distances from the absorbing atoms (i.e., within the ith shell), which are often written as: [31]

$$\chi_i(k) = \frac{S_0^2 n_i}{k R_i^2} \left| f_i^{\text{eff}}(k) \right| \sin \left[2k R_i - \frac{4}{3} \sigma_i^{(3)} k^3 \right.$$
$$\left. + \delta_i(k) \right] e^{-2\sigma_i^2 k^2} e^{-2R_i / \lambda_i(k)}, \quad (1)$$

where k is the photoelectron wave number, $f_i^{\text{eff}}(k)$ and $\delta_i(k)$ are the photoelectron scattering-path amplitude and phase, respectively, S_0^2 is the passive electron reduction factor, n_i is the degeneracy of the scattering path, R_i is the effective half-path length (which equals the interatomic distance for single scattering paths), σ_i^2 is the mean-square deviation in R_i, $\sigma_i^{(3)}$ is the third cumulant of the pair distribution function [32], and $\lambda_i(k)$ is the photoelectron mean free path. The most dominant contribution to the EXAFS signal originates from backscattering of the photoelectron by neighboring atoms toward the absorbing atom ('single scattering'). More complex scattering patterns, known as multiple scatterings (MSs), involve the electron wave's reflections by multiple atoms [33]. The amplitude reduction factor S_0^2 describes the intrinsic losses upon excitation, which arise due to the many-body effects during the photoabsorption process. The scattering amplitudes and phases, along with the photoelectron mean free paths for different scattering configurations contributing to the EXAFS signal, are calculated *ab initio*.

EXAFS analysis is most valuable in the systems where local structure around particular atomic species may deviate from the average, periodic structure (if such exists). Such deviations occur when structural, chemical or thermal disorder is present, such as, for example, in materials with finite sizes in one, two or three dimensions. EXAFS has a distinct advantage over scattering methods because it is (1) element specific and (2) local, that is, probes the environment within 5–8 Å from the central (x-ray absorbing) atom. Hence, an ability to detect strain in nm-scale particles, i.e., below the spatial resolution limit of x-ray and electron diffraction methods, is potentially there. There is also an important difference between the x-ray absorption and (x-ray or electron) scattering methods: the latter probe displacements of atoms
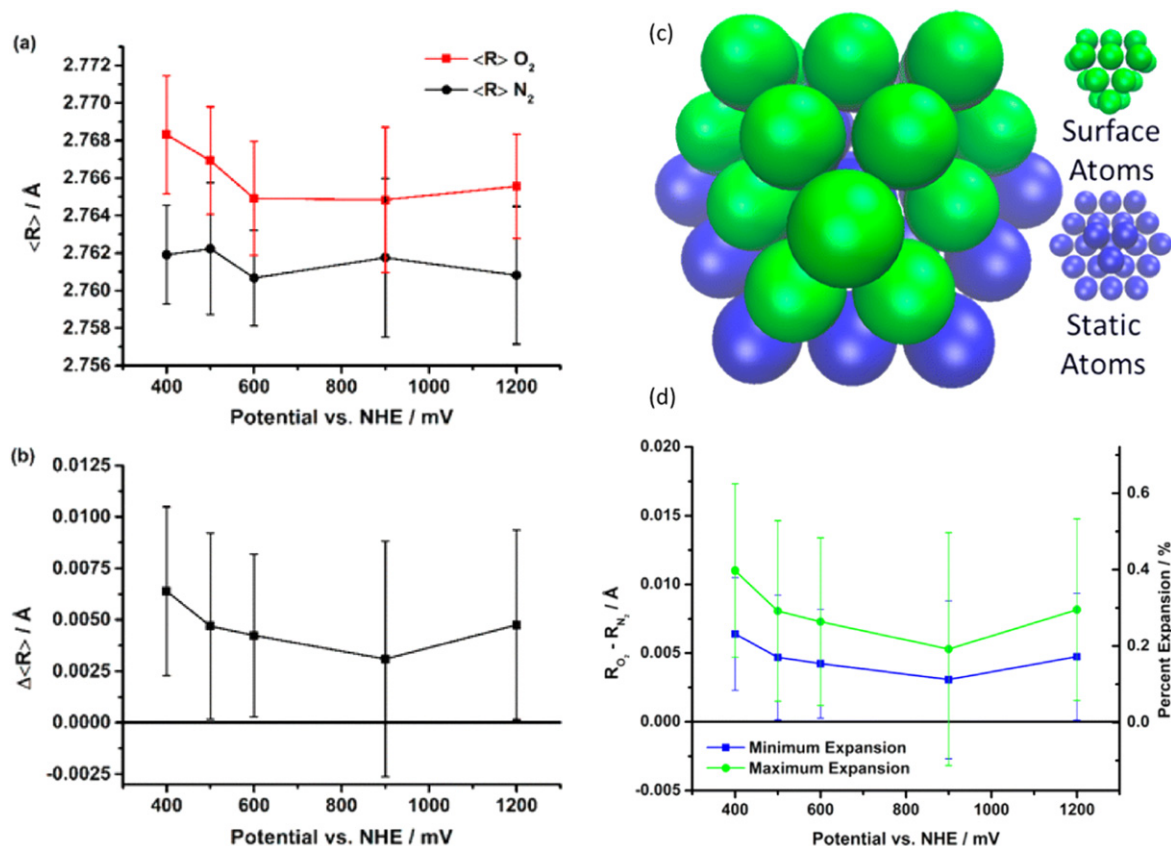
Figure 4. (a) Demonstration of the effect of different atmospheres on the metal–metal bond lengths in nanoparticles. Shown are Pt–Pt bond distances under N_2 and O_2 at three potentials in the double layer region (400 mV, 500 mV, and 600 mV) and at the oxygen reduction reaction onset potential (900 mV) and at an oxidizing potential (1200 mV). (b) Bond length change $\Delta \langle R \rangle$ at all potentials, showing a distinct expansion at all potentials upon exposure to O_2. (c) Depiction of the 37 atom, hemispherically truncated cuboctahedral nanoparticle. This model was used for calculating the maximum, surface-restricted expansion of Pt–Pt bond lengths. The static atoms in the surface-restricted expansion model are represented in blue, whereas the dynamic surface Pt atoms are represented in green. (d) Minimum and maximum Pt–Pt surface bond expansion under O_2 calculated from the ensemble measurement and surface-restricted expansion. Reproduced with permission from [34].

from periodic sites, while the former probe deviations in interatomic bond lengths. Hence, the correlations between individual atom displacements are an integral part of EXAFS measurement. Even within this limitation, as will be shown below, EXAFS can be used to detect strain with greater spatial resolution than scattering techniques. We will now review three distinct modifications of EXAFS analysis that are applicable for strain detection and characterization.

4.1. Direct measurement of bond lengths (R)

Due to the ensemble-averaging nature of EXAFS, determination of surface-specific strain by EXAFS is complicated, but several strategies have been tested recently to isolate the surface contribution to strain from that of the bulk. For example, Erickson *et al*, obtained a change in the Pt–Pt bond length in the nanoparticles in response to the exposure to either O_2 or N_2 gas [34]. In this work, Pt–Pt bond lengths measured in the 1 nm in diameter nanoparticles immobilized in the electrochemical cell were shown to change, depending on the gas flown into the cell (figure 4 (a), (b)). While the distribution of strain within the bonding framework is

impossible to extract from this average method, its upper and lower bounds can be estimated by assuming two extreme models. The 'bulk strain' model corresponds to the uniform bond expansion, where all bonds change by the experimentally observed amount ΔR (figure 4(b)). The second model describes the experimentally observed expansion as the superposition of the two subsets of bonds: the surface ones, expanded, and the rest, unchanged. Using a 35-atom cluster (figure 5(c)) as a simplified model, Ericksen *et al* obtained quantitative estimates of the surface-localized strain. The second model allowed to generate the surface-localized bond expansion, ΔR (figure 5(d)) and the surface-localized strain via:

$$\varepsilon = \frac{\Delta R}{R}, \tag{2}$$

and the stress in the cantilever film, via Stoney's equation. The agreement between the calculated stress–thickness values from EXAFS and from *in situ* cantilever measurements was excellent, thus validating the model used. As in the previous result with melting point suppression in alloys [35], this example highlights a direct link between the microscopic
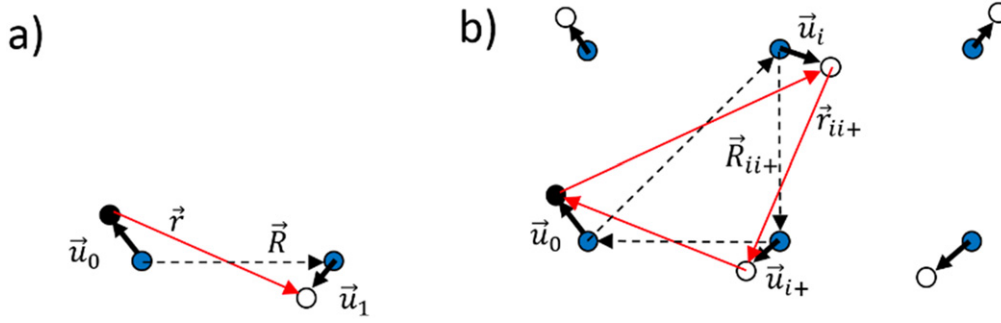
Figure 5. Illustration of the local deviations from the average atomic positions in a lattice and their relationships to the lengths of the single scattering (a) and multiple scattering (b) photoelectron paths. Blue circles indicate periodic lattice sites. Black circles—x-ray absorbing atoms. Open circles: instantaneous positions of atoms that are displaced from the average lattice sites due to either dynamic or static disorder, or both.

strains in nanoparticles measured at the sub-picometer scales and their macroscopic implications (here—on the cantilever measurements).

4.2. Direct measurement of deformation (ΔR) via differential EXAFS

In some cases, the changes in the bond lengths in response to the external perturbation can be measured with much higher accuracy than in the previous method, where actual bond lengths were measured and then subtracted from each other. External perturbations can be introduced by the difference in the *ex situ* treatment conditions [36] or by *in situ* modulation of reactive gas composition [34, 37], electric [38], or magnetic field [39]. In this method, the strain is defined as ΔR, the bond length change between the two structures that underwent different treatments. Conventional analysis methods based on the nonlinear least squares fitting analysis allow to obtain the ΔR values as low as 100 fm, as demonstrated in recent examples [37, 40]. In an exceptional cases of magnetostrictive materials where the strain was measured in response to periodically changing magnetic field, the bond length change of 1 fm was detected. Such accuracy required a unique stability of experimental components and the use of dispersive EXAFS beamline [39]. The sensitivity of EXAFS to structural changes under external conditions can be further enhanced compared to the differential EXAFS analysis by using modulation excitation approach and phase sensitive analysis [41].

4.3. Strain energy via EXAFS Debye Waller factors (σ^2)

EXAFS Debye–Waller factor (σ^2) is defined as the mean square deviation of the half-length of the photoelectron path from the average. In materials with long range periodicity, σ^2 can be related to the local displacements $\vec{u}_i$ from the average lattice sites (figure 5(a)).

For a single scattering photoelectron path, the half path length can be expressed in terms of the length of the vector $\vec{r}$ connecting the instantaneous positions of the absorbing and scattering atoms:

$$\vec{r} = \vec{R} + \vec{u}_1 - \vec{u}_0, \tag{3}$$

where the average leg vector $\vec{R}$ connects two lattice sites that approximate the average positions of the absorber and the scatterer. For a MS path (figure 5(b)), each leg of the path connecting instantaneous atomic positions is given by the vector:

$$\vec{r}_{ii+} = \vec{R}_{ii+} + \vec{u}_{i+} - \vec{u}_i, \tag{4}$$

where, following notation of [42], $i+$ indicates the next neighbor atom to i in the direction of the path, and $\vec{R}_{ii+}$ and $\vec{u}_i$ correspond to the average leg vector and atomic displacement vector, respectively. EXAFS Debye–Waller factor of any scattering path with n legs is defined as:

$$\sigma^2 \equiv \left\langle (r - R)^2 \right\rangle, \tag{5}$$

where the half path lengths of the instantaneous and average paths are:

$$r \equiv \frac{1}{2}\sum_{i=1}^{n} r_{ii+} \text{ and } R \equiv \frac{1}{2}\sum_{i=1}^{n} r_{ii+}. \tag{6}$$

Using equation (4), expression for r_{ii+} can be approximated as: [43]

$$r_{ii+}^2 = \left(\vec{R}_{ii+} + \left(\vec{u}_{i+} - \vec{u}_i\right)\right)^2 \approx R_{ii+}^2 - 2R_{ii+}\hat{R}_{ii+}\left(\vec{u}_i - \vec{u}_{i+}\right),$$

where $\hat{R}_{ii+}$ is a unit vector corresponding to $\vec{R}_{ii+}$. Hence

$$r_{ii+} \approx R_{ii+}\sqrt{1 - 2\frac{\hat{R}_{ii+}}{R_{ii+}}\left(\vec{u}_i - \vec{u}_{i+}\right)} \approx R_{ii+}\left(1 + \frac{\hat{R}_{ii+}}{R_{ii+}}\left(\vec{u}_i - \vec{u}_{i+}\right)\right)$$
$$= R_{ii+} + \left(\vec{u}_i - \vec{u}_{i+}\right)\hat{R}_{ii+}. \tag{7}$$

Incorporating equation (7) into equation (6) we obtain:

$$r \approx R + \frac{1}{2}\sum_{i=1}^{n}\left(\vec{u}_i - \vec{u}_{i+}\right)\hat{R}_{ii+}. \tag{8}$$

From the definition of σ^2 (equation (5)) and equation (8), we obtain: [43]

$$\sigma^2 \approx \left\langle \left(\frac{1}{2} \sum_{i=1}^{n} (\vec{u}_i - \vec{u}_{i+}) \hat{R}_{ii+} \right)^2 \right\rangle$$
$$= \frac{1}{4} \left\langle \left(\sum_{i=1}^{n} (\vec{u}_i - \vec{u}_{i+}) \hat{R}_{ii+} \right)^2 \right\rangle. \qquad (9)$$

For a single scattering path shown in figure 5(a), equation (9) becomes:

$$\sigma^2 \approx \left\langle u_{0x}^2 \right\rangle + \left\langle u_{1x}^2 \right\rangle - 2 \left\langle u_{0x} u_{1x} \right\rangle, \qquad (10)$$

where u_{0x} and u_{1x} are projections of the atomic displacements on the lattice vector $\vec{R}_{01}$, and the last term in equation (10) is the displacement–displacement correlation function. Expressions for EXAFS Debye–Waller factors for MS paths can be easily derived using equation (10) and some of them, for collinear MS paths, can be found in appendix of [43]. This formalism works well for materials where atomic positions are displaced relative to the periodic lattice sites, which is required by equations (3) and (4). In strained nanoparticle surfaces there is no long range periodicity, nor are there periodic sites illustrated in figure 5, hence, the meaning of the vector $\vec{R}_{ii+}$ is lost and equation (3) is not valid, although equation (5) can still be used to characterize strain in the nanoparticle. It is because of the displacement–displacement correlation term in equation (10) that the bond length disorder cannot be simply related to the superposition of the two atom displacements, the central atom one and its nearest neighbor.

In addition to strain measurements, EXAFS analysis allows evaluating energetic characteristics associated with local deformations of interatomic bonds. In elastic approximation, local strain energy averaged over the ensemble of bonds can be calculated by EXAFS, as was done, e.g., in [35] and, later, modified in [6]:

$$U = \frac{1}{2} N k \sigma^2. \qquad (11)$$

Here U is the total elastic energy per atom, N is the metal–metal (M–M) coordination number, k is the force constant of the M–M bond, and σ^2 is the mean square bond length disorder. In the harmonic approximation, the force constant is: $k = \mu \omega^2$, where $\mu = m/2$ is the reduced mass of the M–M bond, $\omega = k_B \Theta_E / \hbar$ is the Einstein frequency, $\hbar$ is Planck's constant and Θ_E is the Einstein temperature. When static (temperature independent) strain is present, equation (11) can be written as the sum of two contributions: $U = V(T) + W$, where $V(T)$ arises due to dynamic vibrations, and W originates from the static disorder present in the system of interatomic bonds. These two terms can be separately evaluated by expressing σ^2 in terms of the dynamic and static terms (σ_d^2 and σ_s^2, respectively) of the EXAFS Debye–Waller factor σ_{st}^2:

$$\sigma^2 = \sigma_d^2 + \sigma_s^2. \qquad (12)$$

The residual elastic strain energy due to the static disorder is then identifiable as simply: [6]

$$U_s = \frac{1}{2} N k \sigma_s^2. \qquad (13)$$

In harmonic approximation, the force constant k can be found from the Einstein temperature measurement within the same EXAFS experiment. Equation (13) can be used in for a wide range of materials, from bulk to nanoscale, as long as the coordination numbers of particular species and their dynamic characteristics are known. As shown many times in EXAFS analysis, the local distortions from the average structure, obtained at the length scale of just a few interatomic distances around atomic species may be important for explaining materials properties at much larger length scales. For example, in [35], it was demonstrated that the residual strain energy due to the bond length mismatch in bulk binary alloys maximized in the middle of the concentration range, and was sufficiently large to explain the melting point suppression of the alloys. X-ray powder diffraction measurements confirmed the existence of microstrain in binary alloys and provided independent estimate of the energy associated with the microstrain, showing that it is the important factor in thermal instability of the disordered phase of Au–Cu alloys at low temperatures [44, 45]. In [6], it was shown that the strain energy of nm-scale metal catalysts is of the same order of magnitude with the chemisorption energy of adsorbates, and, hence, should be taken into account in fundamental theories of reactivity of nanocatalysts.

5. Artifacts of EXAFS analysis and correction strategies

Surface strain of nanoparticles causes data analysis artifacts if the bond length distribution is strongly asymmetric, and special care is needed to reliably extract the structural information from the data. Small (1–5 nm) metal clusters may undergo significant surface reconstruction under the influence of ligands and/or substrate. During such processes the most affected are the atoms on the periphery of the clusters. Hence, the pair distribution function, that includes the contributions of surface and interior atoms, will be skewed from the symmetric shape that is typical for relatively ordered materials or those with a strong but uniform disorder. Such asymmetric disorder was observed in the clusters probed by coherent electron scattering by Huang *et al* [2]. Assuming a model with variable radial distortion that matches data of [2], Yevick and Frenkel [46] showed that the bond length distribution in the clusters studied by Huang *et al*, is strongly asymmetric (figure 6).

They generated theoretical EXAFS signal using such asymmetrically distorted clusters and demonstrated that conventional data analysis procedures based on quasi-Gaussian approximation of disorder and nonlinear least square refinement methods result in underestimation of the coordination numbers and bond length disorders [46]. The inability of EXAFS analysis to correctly detect strongly and
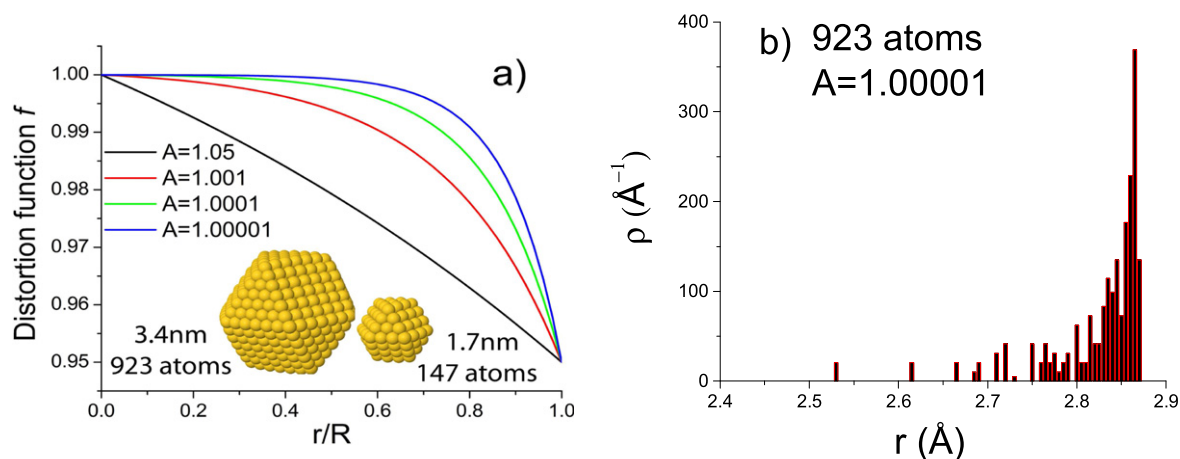
Figure 6. (a) Distortion functions applied to the regular truncated cuboctahedral clusters to produce symmetric and asymmetric (b) bond length distributions (reproduced with permission from [46]).
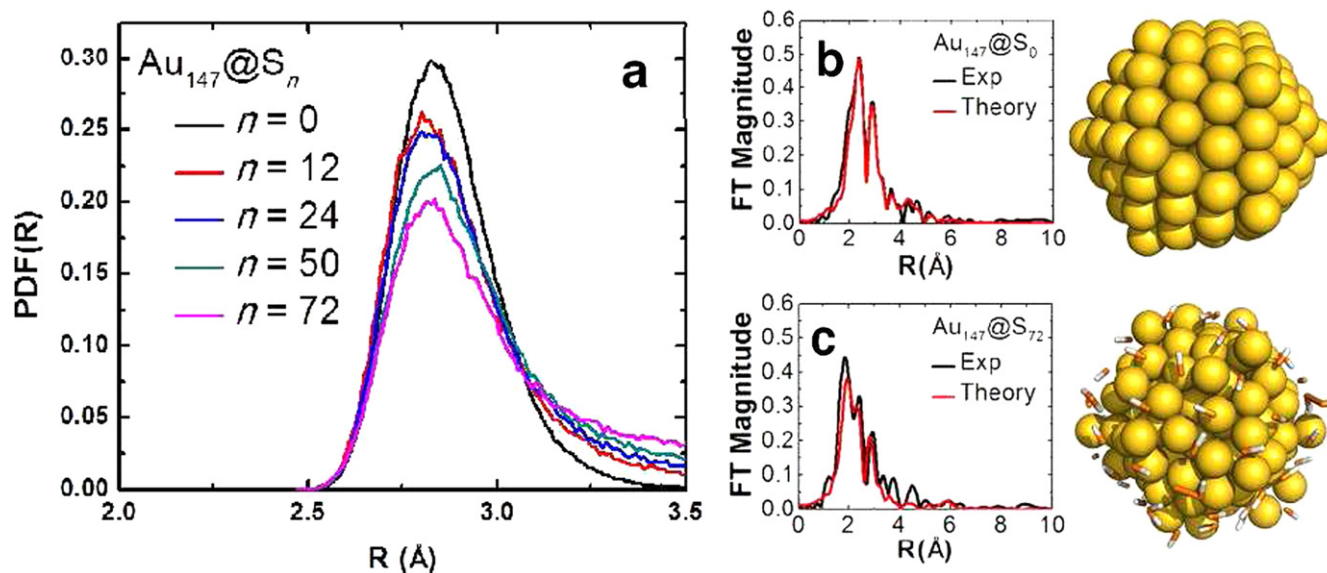

Figure 7. (a) First shell Au–Au PDFs calculated using 200 independent snapshots from the DFT-MD simulations. Comparisons of experimentally and theoretically derived EXAFS data in *R*-space: (b) $Au_{147}@S_0$ and (c) $Au_{147}@S_{72}$. Representative snapshots of the DFT-MD trajectories taken from the portion of the simulations used to calculate the respective theoretical EXAFS signals and PDFs. Reproduced with permission from [50].

asymmetrically distorted subsets of bonds is thus a matter of concern for a large class of nanomaterials such as catalysts that are prone to exactly this type of distortions, but how important these corrections are for particles of different elements, sizes, shapes and details of their environment is a subject of ongoing research. Recently, direct modeling approaches based on the first principle calculations using density functional theory (DFT) and molecular dynamics (MD) were proposed as an alternative to inverse analysis approach such as fitting [47–51]. Using the direct modeling of EXAFS spectra on DFT/MD-optimized cluster configurations, the configuration- and time- average EXAFS spectra of disordered clusters were obtained, that contain almost no adjustable parameters. Such spectra can be directly compared with experiment and, if the agreement is satisfactory, atomic configurations of the simulated clusters can be used for

structural analysis (figure 7) [50]. This approach is thus similar to that used by Huang *et al*, where theoretical calculations of atomic positions were used to construct electron diffraction coherent scattering pattern in strained 4 nm-Au clusters and compare with experimental data [2].

6. Concluding remarks

The quest for solving the structure of metal clusters brings two synchrotron communities, the scattering and spectroscopy ones, in front of the same closed door. Behind that door is a mystery, a disordered metal cluster of a couple nanometers in size that eludes any attempt of direct imaging. In front are two different types of researchers that were historically quite independent from each other, each with their own

'temptations' [14]. For x-ray diffraction, the cluster is too small for 3D refinement. For x-ray absorption spectroscopy, ensemble-averaging of the results obtained by relatively large beams lowers the quantitative capability of the method. With the development of nm-focusing optics and powerful x-ray sources that generate high-flux, coherent beams, a new opportunity will emerge for both scattering and spectroscopy to bridge this gap and characterize the same object, a single metal cluster of nanometer dimensions.

Acknowledgments

References

[1] Harder R and Robinson I 2013 Coherent x-ray diffraction imaging of morphology and strain in nanomaterials *JOM* **65** 1202

[2] Huang W J, Sun R, Tao J, Menard L D, Nuzzo R G and Zuo J M 2008 Coordination-dependent surface atomic contraction in nanocrystals revealed by coherent diffraction *Nat. Mater.* **7** 308

[3] Frenkel A I, Cason M W, Elsen A, Jung U, Small M W, Nuzzo R G, Vila F D, Rehr J J, Stach E A and Yang J C 2014 Critical review: effects of complex interactions on structure and dynamics of supported metal catalysts *J. Vac. Sci. Technol.* A **32** 020801

[4] Frenkel A I, Small M W, Smith J G, Nuzzo R G, Kvashnina K O and Tromp M 2013 An *in situ* study of bond strains in 1 nm Pt catalysts and their sensitivities to cluster–support and cluster–adsorbate interactions *J. Phys. Chem.* C **117** 23286

[5] Small M W, Kas J J, Kvashnina K O, Rehr J J, Nuzzo R G, Tromp M and Frenkel A I 2014 Effects of adsorbate coverage and bond-length disorder on the d-band center of carbon-supported Pt catalysts *ChemPhysChem* **15** 1569

[6] Small M W, Sanchez S I, Marinkovic N S, Frenkel A I and Nuzzo R G 2012 Influence of adsorbates on the electronic structure, bond strain, and thermal properties of an alumina-supported Pt catalyst *ACS Nano* **6** 5583

[7] Li L *et al* 2013 Noncrystalline-to-crystalline transformations in Pt nanoparticles *J. Am. Chem. Soc.* **135** 13062

[8] Amakawa K *et al* 2013 How strain affects the reactivity of surface metal oxide catalysts *Angew. Chem. Int. Ed.* **52** 13553

[9] Strasser P *et al* 2010 Lattice-strain control of the activity in dealloyed core–shell fuel cell catalysts *Nat. Chem.* **2** 454

[10] Zhang S *et al* 2014 Tuning nanoparticle structure and surface strain for catalysis optimization *J. Am. Chem. Soc.* **136** 7734

[11] Kuo C-H *et al* 2013 The effect of lattice strain on the catalytic properties of Pd nanocrystals *ChemSusChem* **6** 1993

[12] Mavrikakis M, Hammer B and Nørskov J K 1998 Effect of strain on the reactivity of metal surfaces *Phys. Rev. Lett.* **81** 2819

[13] Pratt A *et al* 2014 Enhanced oxidation of nanoparticles through strain-mediated ionic transport *Nat. Mater.* **13** 26

[14] Stoneham A M and Gavartin J L 2007 Dynamics at the nanoscale *Mater. Sci. Eng.* C **27** 972

[15] Robinson I K and Vartanyants I A 2001 Use of coherent x-ray diffraction to map strain fields in nanocrystals *Appl. Surf. Sci.* **182** 186

[16] Cha W *et al* 2010 Exploration of crystal strains using coherent x-ray diffraction *New J. Phys.* **12** 035022

[17] Pfeifer M A, Williams G J, Vartanyants I A, Harder R and Robinson I K 2006 Three-dimensional mapping of a deformation field inside a nanocrystal *Nature* **442** 63

[18] Bates R H T 1982 Fourier phase problems are uniquely soluble in more than one dimension: I. Underlying theory *Optik* **61** 247

[19] Miao J, Sayre D and Chapman H N 1998 Phase retrieval from the magnitude of the Fourier transforms of nonperiodic objects *J. Opt. Soc. Am.* A **15** 1662

[20] Robinson I K, Vartanyants I A, Williams G J, Pfeifer M A and Pitney J A 2001 Reconstruction of the shapes of gold nanocrystals using coherent x-ray diffraction *Phys. Rev. Lett.* **87** 195505

[21] Baruchel J *et al* 2006 Advances in synchrotron radiation microtomography *Scr. Mater.* **55** 41

[22] Riekel C 2000 New avenues in x-ray microbeam experiments *Rep. Prog. Phys.* **63** 233

[23] Harder R, Pfeifer M A, Williams G J, Vartaniants I A and Robinson I K 2007 Orientation variation of surface strain *Phys. Rev.*B **76** 115425

[24] Rau C, Crecea V, Liu W, Richter C P, Peterson K M, Jemian P R *et al* 2007 Synchrotron-based imaging and tomography with hard x-rays *Nucl. Instrum. Methods Phys. Res.* B **261** 850

[25] Robinson I and Harder R 2009 Coherent x-ray diffraction imaging of strain at the nanoscale *Nat. Mater.* **8** 291

[26] Frenkel A I, Hills C W and Nuzzo R G 2001 A view from the inside: complexity in the atomic scale ordering of supported metal nanoparticles *J. Phys. Chem.* B **105** 12689

[27] Frenkel A I 1999 Solving the structure of nanoparticles by multiple-scattering EXAFS analysis *J. Synchrotron Radiat.* **6** 293

[28] Frenkel A 2007 Solving the 3D structure of metal nanoparticles *Z. Kristallogr.* **222** 605

[29] Frenkel A I 2012 Applications of extended x-ray absorption fine-structure spectroscopy to studies of bimetallic nanoparticle catalysts *Chem. Soc. Rev.* **41** 8163

[30] Sayers D E, Stern E A and Lytle F W 1971 New technique for investigating noncrystalline structures: fourier analysis of the extended x-ray absorption fine structure *Phys. Rev. Lett.* **27** 1204

[31] Zabinsky S I, Rehr J J, Ankudinov A, Albers R C and Eller M J 1995 Multiple-scattering calculations of x-ray-absorption spectra *Phys. Rev.* B **52** 2995

[32] Bunker G 1983 Application of the ratio method of EXAFS analysis to disordered systems *Nucl. Instrum. Methods* **207** 437

[33] Rehr J J and Albers R C 2000 Theoretical approaches to x-ray absorption fine structure *Rev. Mod. Phys.* **72** 621

[34] Erickson E M *et al* 2014 A comparison of atomistic and continuum approaches to the study of bonding dynamics in electrocatalysis: microcantilever stress and *in situ* EXAFS observations of platinum bond expansion due to oxygen adsorption during the oxygen reduction reaction *Anal. Chem.* **86** 8368

[35] Frenkel A, Stern E, Voronel A and Heald S 1996 Lattice strains in disordered mixed salts *Solid State Commun.* **99** 67

[36] Frenkel A I *et al* 2012 Thermal properties of nanoporous gold *Phys. Rev.* B **85** 195419

[37] Spanjers C S, Senftle T P, van Duin A C, Janik M J, Frenkel A I and Rioux R M 2014 Illuminating surface atoms in nanoclusters by differential x-ray absorption spectroscopy *Phys. Chem. Chem. Phys.* **16** 26528

[38] Korobko R, Lerner A, Li Y, Wachtel E, Frenkel A I and Lubomirsky I 2015 *In-situ* extended x-ray absorption fine structure study of electrostriction in Gd doped ceria *Appl. Phys. Lett.* **106** 042904

[39] Pettifer R F, Mathon O, Pascarelli S, Cooke M D and Gibbs M R J 2005 Measurement of femtometre-scale atomic displacements by x-ray absorption spectroscopy *Nature* **435** 78

[40] König C F J, van Bokhoven J A, Schildhauer T J and Nachtegaal M 2012 Quantitative analysis of modulated excitation x-ray absorption spectra: enhanced precision of EXAFS fitting *J. Phys. Chem.* C **116** 19857

[41] Chiarello G L and Ferri D 2015 Modulated excitation extended x-ray absorption fine structure spectroscopy *Phys. Chem. Chem. Phys.* **17** 10579

[42] Poiarkova A V and Rehr J J 1999 Multiple-scattering x-ray-absorption fine-structure Debye-Waller factor calculations *Phys. Rev.* B **59** 948

[43] Shanthakumar P *et al* 2006 X-ray study of the ferroelectric $[Ba_{0.6}Sr_{0.4}][(YTa)_{0.03}Ti_{0.94}]O_3$ *Phys. Rev.* B **74** 174103

[44] Rosenberg Y *et al* 2000 Strain energy density in the x-ray powder diffraction from mixed crystals and alloys *J. Phys.: Condens. Matter.* **12** 8081

[45] Machavariani V S *et al* 2001 Local disorder in mixed crystals as viewed by XRPD *AIP Conf. Proc.* **554** 521

[46] Yevick A and Frenkel A I 2010 Effects of surface disorder on EXAFS modeling of metallic clusters *Phys. Rev.* B **81** 115451

[47] Vila F, Rehr J J, Kas J, Nuzzo R G and Frenkel A I 2008 Dynamic structure in supported Pt nanoclusters: real-time density functional theory and x-ray spectroscopy simulations *Phys. Rev.* B **78** 121404

[48] Roscioni O M, Zonias N, Price S W T, Russell A E, Comaschi T and Skylaris C-K 2011 Computational prediction of L_3 EXAFS spectra of gold nanoparticles from classical molecular dynamics simulations *Phys. Rev.* B **83** 115409

[49] Price S W T, Zonias N, Skylaris C-K, Hyde T I, Ravel B and Russell A E 2012 Fitting EXAFS data using molecular dynamics outputs and a histogram approach *Phys. Rev.* B **85** 075439

[50] Yancey D F, Chill S T, Zhang L, Frenkel A I, Henkelman G and Crooks R M 2013 A theoretical and experimental examination of systematic ligand-induced disorder in Au dendrimer-encapsulated nanoparticles *Chem. Sci.* **4** 2912

[51] Chill S T, Anderson R M, Yancey D F, Frenkel A I, Crooks R M and Henkelman G 2015 Probing the limits of conventional extended x-ray absorption fine structure analysis using thiolated Au nanoparticles *ACS Nano* **9** 4036–42